

# Effect of Plasma Treatment on Metal Oxide p–n Thin Film Diodes Fabricated at Room Temperature

Yin Jou Khong, Kham Man Niang,\* Sanggil Han, Nigel J. Coburn, Gwenhivir Wyatt-Moon, and Andrew J. Flewitt

There is a need for a good quality thin film diode using a metal oxide p–n heterojunction as it is an essential component for the realization of flexible large-area electronics. However, metal oxide-based diodes normally show poor rectification characteristics whose origin is still poorly understood; this is holding back their use in various applications. A systematic study of the origins of the poor performance is performed based on bias-stress measurements using a cuprous oxide (Cu<sub>2</sub>O)/amorphous zinc-tin oxide (a-ZTO) heterojunction as an example. This suggests that multiple carrier trapping and thermal release of carriers in defect states stemming from oxygen vacancies at the heterojunction interface is the primary cause of poor rectification. It is demonstrated that a plasma treatment is an effective way to optimize the population of oxygen vacancies at the heterojunction interface based on extensive material analyses, allowing a significant improvement in the diode performance with a much-enhanced rectification ratio from ≈20 to 10 000, and a consequent facilitation of the next-generation of ubiquitous electronics.

In addition to metal oxide TFTs that have been extensively researched, metal oxide p–n junction diodes are important components for the realization of flexible and low cost large-area electronics. For example, diode rectifiers are particularly useful in a variety of flexible electronic applications, including solar cells, emerging wireless power transmission technology, and radio-frequency identification tags.<sup>[2,3]</sup> The metal oxide p–n diodes fabricated at room temperature still retains good electronic properties and can be deposited on a wide variety of substrates that are otherwise unsuitable for high temperature processing, thus improving the ease of integration of electronics.

Heterojunction diodes using combinations of various n-type and p-type oxide materials have been reported. For the n-type materials, both tertiary and quater-

nary oxides of zinc are available. This is because the introduction of extra elements improves the electronic characteristics of the zinc oxide (ZnO), such as increased mobility and free carrier suppression by indium and gallium respectively in a-IGZO<sup>[4–6]</sup>. While a-IGZO has been most widely used, other materials such as amorphous zinc tin oxide (a-ZTO) and indium zinc oxide (IZO) have also been reported.<sup>[5,7]</sup> Alternative n-type materials composed of abundant elements are needed for sustainable low-cost production; a-ZTO is such candidate as it also exhibits promising electronic properties such as a high electron mobility (>10 cm<sup>2</sup> V<sup>-1</sup> s<sup>-1</sup>).<sup>[8,9]</sup> For the p-type materials, binary compounds such as cuprous oxide (Cu<sub>2</sub>O) and nickel oxide (NiO) provide relatively simpler process parameters compared to ternary oxide compounds like the spinels. Furthermore, the binary p-type materials are well known to have intrinsically stable p-type conductivity due to the ease of formation of native acceptors with a shallow energy level in the band gap.<sup>[10,11]</sup> In particular, Cu<sub>2</sub>O has been recognized as a promising p-type oxide for a long time, with the valence band maximum mainly consisting of hybridized Cu 3d- and O 2p-orbitals, providing a less localized hole transport pathway.<sup>[12]</sup>


Most of the metal oxide diodes reported are fabricated at relatively high temperatures.<sup>[13–16]</sup> For example, p-SrCu<sub>2</sub>O<sub>2</sub>/n-ZnO:Al diodes reported by Kim et al., where the thin films are deposited at 400–500 °C by sputtering, exhibit a rectification ratio of ≈7 at ±5 V.<sup>[17]</sup> On the other hand, Schein et al. used pulsed laser deposition (PLD) at 650 °C to produce p-ZnCo<sub>2</sub>O<sub>4</sub>/n-ZnO diodes, exhibiting very high rectification ratio of 2 × 10<sup>10</sup> at ±2 V.<sup>[18]</sup> Recently, there have been

## 1. Introduction

Thin film oxide semiconductors have been a topic of significant interest in the field of large area electronics since the first demonstration of amorphous indium–gallium–zinc oxide (a-IGZO) thin film transistors (TFTs) fabricated at low temperatures.<sup>[1]</sup> This is because amorphous oxide semiconductors (AOSs) provide not only good electronic properties even when they are deposited at room temperature, allowing the use of low-temperature or flexible substrates, but also excellent uniformity for large area electronics as a result of their amorphous structure.

Y. J. Khong, Dr. K. M. Niang, Dr. S. Han, Dr. N. J. Coburn, Dr. G. Wyatt-Moon, Prof. A. J. Flewitt  
Electrical Engineering Division  
University of Cambridge  
9 J J Thomson Avenue, Cambridge CB3 0FA, UK  
E-mail: kmn36@cam.ac.uk

Dr. N. J. Coburn  
College of Engineering  
Boston University  
44 Cummington Mall, Boston, MA 02215, USA

 The ORCID identification number(s) for the author(s) of this article can be found under <https://doi.org/10.1002/admi.202100049>.

© 2021 The Authors. Advanced Materials Interfaces published by Wiley-VCH GmbH. This is an open access article under the terms of the Creative Commons Attribution License, which permits use, distribution and reproduction in any medium, provided the original work is properly cited.

DOI: 10.1002/admi.202100049

a few reports on room-temperature processed metal oxide heterojunction diodes showing high performance.<sup>[2,3,19,20]</sup> For example, a p-Cu<sub>2</sub>O/n-IGZO diode by room-temperature sputtering is reported to show a rectification ratio of  $3.4 \times 10^4$  at  $\pm 1.2$  V.<sup>[3]</sup> Another diode made from p-NiO<sub>x</sub>/n-ZnO exhibiting a rectification ratio of  $2 \times 10^{10}$  at  $\pm 2$  V was also fabricated using PLD.<sup>[21]</sup> Whilst PLD allows all target components to be ejected equally irrespective of their binding energies, it is hard to scale up as required for large electronics manufacture as it suffers from lower film uniformity and smaller deposition area compared to sputtering, both of which are crucial.<sup>[22]</sup>

One method to improve the performance of thin film diodes is to insert an “intrinsic” layer between the p- and n-type oxides, as demonstrated by Schlupp et al. in p-ZnCo<sub>2</sub>O<sub>4</sub>/n-ZTO diodes, which are the best heterojunction diodes reported so far with a rectification over  $10^6$  and ideality factors close to 1.<sup>[20]</sup> The addition of an interface material complicates fabrication, but it illustrates the importance of interface conditions of the p–n heterojunction in diode performance.

In this work, we set out to fabricate heterojunction diodes using only abundant materials: zinc, tin, and copper. This is achieved with n-type a-ZTO (Zn<sub>x</sub>Sn<sub>1-x</sub>O<sub>y</sub>) and an intrinsically stable p-type Cu<sub>2</sub>O, both of which are processed at room temperature by magnetron sputtering, except for baking during photolithography (at 110–120 °C for 60–120 s). The motivation for room temperature processing is due to its low cost, possibility of using flexible substrates, and ease of integration in electronic circuits. The specific combination of a-ZTO and Cu<sub>2</sub>O is chosen due to their composition of more abundant elements compared to, for example, indium and gallium from a-IGZO. In addition, it is found that a Cu<sub>2</sub>O/a-ZTO p–n heterojunction shows great potential after an extensive review of literature, but it still remains largely unexplored. In particular, we investigate the effect of a simple plasma treatment at the interface between the a-ZTO and Cu<sub>2</sub>O and demonstrate that it significantly improves their rectification performance. The main reason for this is attributed to the interface quality of the junction, as shown by extensive analyses of current–voltage (*I*–*V*) and capacitance–voltage (*C*–*V*) characteristics, and supported by material characterizations including scanning electron microscopy (SEM), Hall effect measurements, and X-ray photoemission spectrum (XPS). In this paper, we first present the untreated heterojunction diodes and investigation on its carrier transport mechanism by bias and temperature treatments. Next, we present the effect of various plasma treatments at the interface and the improved electronic properties. Finally, we compare our data with a few notable results that have been published previously.

## 2. Results and Discussion

### 2.1. Untreated Heterojunction Diodes

The structure of the fabricated heterojunction diode is a very simple sandwich configuration, with a bottom molybdenum (Mo) contact, p–n junction layers (a-ZTO followed by Cu<sub>2</sub>O), and a top gold (Au) contact (Figure 1a). The cross-sectional scanning electron micrograph in Figure 1a shows that both a-ZTO and Cu<sub>2</sub>O films are compact and free of voids, and a clean and smooth interface is formed between the two layers. The crystal-

lographic property of these films has been confirmed by X-ray diffraction in previous reports.<sup>[9,23]</sup> The metal–semiconductor junctions of Au/Cu<sub>2</sub>O and Mo/a-ZTO that form the contacts to the diodes have been confirmed to be Ohmic. Therefore, any non-Ohmic behavior can be attributed to the semiconductor junction. Initially, both configurations with the n-type material on top of the p-type (n-on-p) and vice versa (p-on-n) were considered, but only the latter form rectifying junctions.

As shown in Figure 1b, the untreated diode exhibits a good *I*–*V* response, with a sharp exponential turn-on in forward bias region at  $\approx 0.5$  V and a small reverse saturation current density ( $\approx 3 \times 10^{-2}$  A cm<sup>-2</sup>). The diode rectification ratio is  $\approx 20$ , and the ideality factor of the *I*–*V* curves is about 6.45, extracted based on the Shockley diode equation taking into account parasitic resistances,

$$I = I_0 \left[ \exp \left( \frac{q \{V - R_s I\}}{\eta k T} \right) - 1 \right] + \frac{V - R_s I}{R_p} \quad (1)$$

where *q* is the electronic charge, *V* is the applied voltage, *I* is the measured current, *k* is the Boltzmann constant, *T* is the temperature,  $\eta$  is the ideality factor, and *R<sub>s</sub>* and *R<sub>p</sub>* are the parasitic series and parallel resistances of the diode and its contacts, respectively. Note that a sweep going from negative to positive voltages applied to the p-side is done first, followed by positive to negative sweep; this applies to all the *I*–*V* measurements in this work. The presence of a depletion region, which is crucial for a junction diode, is verified with a *C*–*V* measurement, illustrated in Figure 1c. Figure 1c also shows very large hysteresis of the *C*–*V* curve, indicating a significantly large trap concentration at the interface. Figure S1, Supporting Information, illustrates the frequency dependence of the *C*–*V* response of the untreated diode, which may be interpreted as a further sign of interfacial traps. The presence of an interface dipole is ruled out as there is no noticeable voltage shift in the *I*–*V* response of the diode between sweeps. The built-in voltage is 0.08 V at 100 kHz, extracted from the *x*-intercept of the linear *C*<sup>-2</sup>–*V* plot.

The reverse current density reaches a magnitude of 30 mA cm<sup>-2</sup> at  $-1.0$  V, which is relatively small compared to the forward current density of 420 mA cm<sup>-2</sup> at 1.0 V, but is still significantly high for a reverse bias region where the reverse current density for an oxide thin film diode is reported to be as low as 7 nA cm<sup>-2</sup>.<sup>[20]</sup> It is possible that there are defects in the depletion layer resulting in leakage current paths, which may be eliminated by interface treatments.<sup>[19]</sup>

Next, the carrier transport mechanism is investigated by *I*–*V* measurements at controlled temperatures between 30 and 60 °C. Figure 2a shows the diode’s *I*–*V* response which are labeled as “pre-stress” to distinguish them from the bias stress measurements shown later. For the forward bias (0 to 1 V), the current in positive to negative (downward) sweep exhibits a higher value than the negative to positive (upward) sweep (hysteresis); and that is true for all the temperature range used here. This suggests that there are some trap states which are being filled as the positive voltage is applied. At rest, the density of states in the a-ZTO layer is in a state of equilibrium where there is a certain distribution of electron-filled and ionized oxygen vacancy states. When an applied forward bias reduces the depletion width, the process of converting ionized oxygen vacancies to electron-filled state is favored, reducing electron

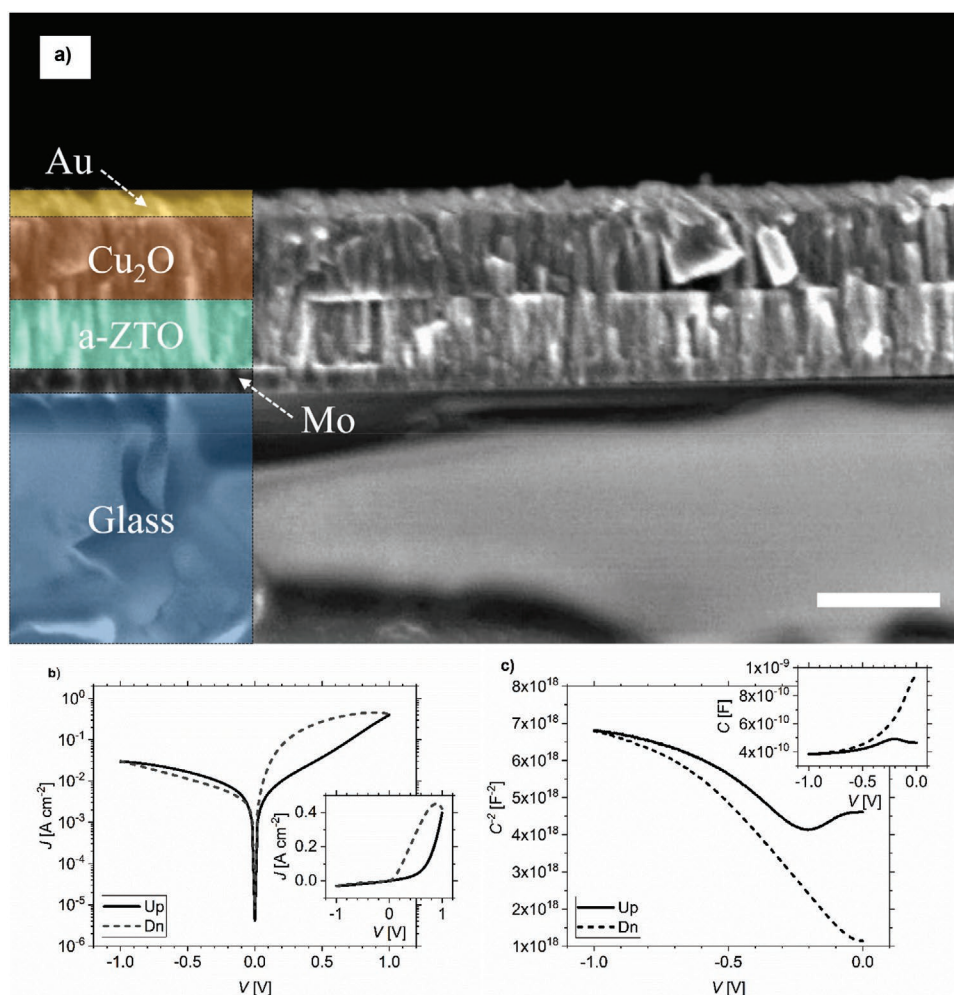


**Figure 1.** a) Cross sectional SEM micrograph of heterojunction diode structure, with schematic overlay to indicate each layer (scale bar: 500 nm), b)  $I$ - $V$  and c)  $C$ - $V$  response of untreated diode with alternating current (AC) signal at 100 kHz. Upward (Up) sweep indicates increasingly positive applied bias during measurement and downward (Dn) sweep indicates increasingly negative applied voltage. Upward sweeps are done before downward sweeps throughout this work.

traps in the band gap. Moreover, the forward current increases significantly with temperature, by a factor of  $\approx 30$

and  $60^\circ\text{C}$ , increasing the calculated rectification ratios from  $\approx 6$  at  $30^\circ\text{C}$  to  $\approx 50$  at  $60^\circ\text{C}$ .

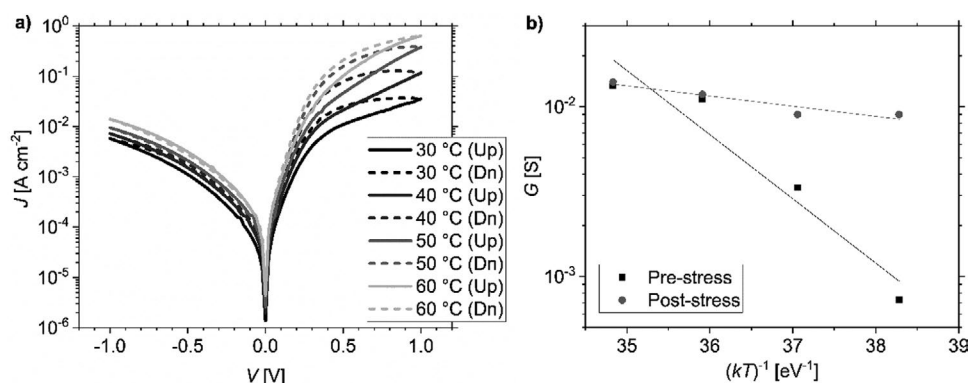


**Figure 2.** a)  $I$ - $V$  response of untreated diode at several temperatures pre-stress. b) Arrhenius plot of untreated diode comparing pre-stress and post-stress conductance at an applied bias of 1 V.

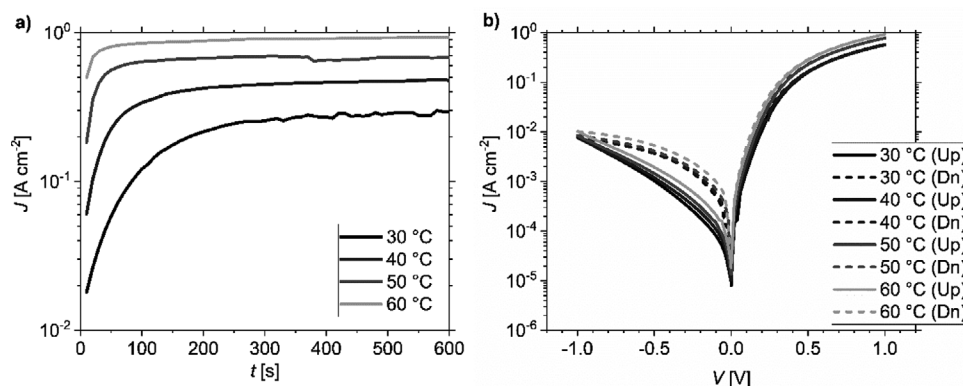


**Figure 3.** a) Bias stress measurements of the untreated diode with a forward bias of 1 V. b)  $I$ - $V$  response of the untreated diode at several temperatures post-stress.

An Arrhenius plot is done with only datapoints from negative to positive sweeps as shown in Figure 2b. The activation energy extracted from the slope of a linear fit of the Arrhenius plot is 0.87 eV. This could mean that the defect states centered around 0.7 eV below the conduction band as reported by Erslev et al. must be fully occupied before the Fermi level can get to the mobility edge.<sup>[24,25]</sup> It is therefore plausible that the untreated diode exhibits trap-limited conduction at large forward bias; this also supports the explanation for the difference between negative to positive and positive to negative sweeps observed in Figure 2a.

To further investigate the conduction processes at the junction, the untreated diode was put through a bias-stress measurement in the dark. As a first test, a forward bias stress of 1.0 V was applied across the diode for 10 min and the current flowing through the device was constantly recorded (Figure 3a). At 30 °C, the diode forward current rises significantly initially but saturates at  $\approx 400$  s. At higher temperatures, the time it takes for the current to saturate decreases. Next, the tests were repeated with a longer bias stress of 4 h and the  $I$ - $V$  measurements were taken at the end (labeled as “post-stress” in Figure 3b). It is found that with the positive bias (0 to 1 V), the current slightly increases with temperature, by a factor of  $\approx 2$  between 30 and 60 °C. Moreover, negligible hysteresis is observed (similar current between forward and reverse sweeps). On the contrary, with the negative bias (0 to  $-1$  V), the current is significantly higher in the down sweep than in the up sweep (large hysteresis). The “post-stress” rectification at 60 °C is calculated to be  $\approx 100$ , twice of the “pre-stress” rectification (in Figure 2a). It is also very interesting to note that the hysteresis appears in the forward bias region (positive applied voltage, Figure 2a) in the “pre-stress” devices, whereas in the “post-stress” devices, the hysteresis appears in the reverse bias region (negative applied voltage, Figure 3b); this is discussed next. Finally, it should be noted that the devices were reset to their initial states by annealing at 150 °C for 20 min before repeating between different temperatures/bias stressing.

These stressing effects can be attributed to a trapping and release of charge at defects that are at or close to the junction interface. The traps capture the mobile charge carriers which should form the current flow across the diode. Before stressing, the traps were mostly empty, and any mobile charges that were

captured by these traps require a minimum activation energy in order to escape. In this analysis, the extra energy was provided in the form of heat. The carriers were able to escape more easily upon trapping at higher temperature, resulting in more of them contributing to the current, hence the larger forward current density at a higher temperature (Figure 3b). In the reverse bias region of the pre-stress curve in Figure 2a, as most traps are already empty, the reverse bias would just enlarge the depletion region by evacuating any mobile charges near the interface resulting in very little hysteresis. In contrast, in the post-stress situation of Figure 3b, as most of the traps were filled to begin with, the reverse bias region caused a large hysteresis in the  $I$ - $V$  response, with negligible hysteresis in the forward bias region. The origin of such trap states could be caused by the local arrangement, defect migration, and shifting energetic positions of the cations, oxygen ions and vacancies, as various authors have suggested in their respective works.<sup>[26–31]</sup>

In addition, the activation energy of conduction is also very different between “pre-stress” and “post-stress”: 0.87 and 0.14 eV respectively (Figure 2b). Erslev et al. reported an unoccupied defect distribution positioned about 0.1 eV below the mobility gap, hence these may be the shallower traps that exhibited the 0.14 eV activation as shown here, after the deeper traps have been completely occupied after bias stress.<sup>[24]</sup> This would be consistent with the untreated diode still retaining the filled traps long enough for the measurements until thermal annealing was done. During bias stress, these deep traps were filled completely. Due to their large activation energy, they could not release their trapped charges as easily and so stay filled for a longer period. As the trap states get filled up, the energy distance between the filled traps and transport states reduces, hence the activation energy shows a decreasing trend.<sup>[32]</sup>

## 2.2. Heterojunction Diodes with Interface Plasma Treatment

Since the results of untreated diode all point towards abundance of some form of trap states near or at the interface, it is imperative to reduce these trap states in order to improve the overall performance of the diodes. It is reported that oxygen treatment of the surface of the metal oxide or certain metal contacts before the deposition of the next layer of material can

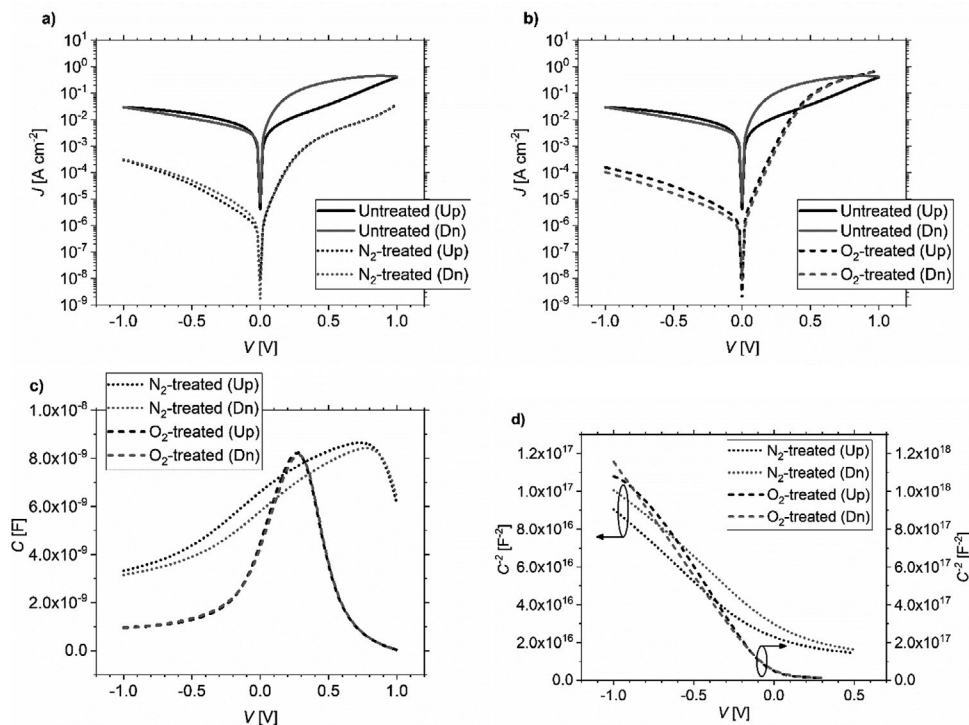


**Figure 4.** Comparison of  $I$ - $V$  responses of a) untreated against nitrogen-treated diode and b) untreated against oxygen-treated diode. c,d) Comparison of  $C$ - $V$  responses of nitrogen-treated diode against oxygen-treated diode.

benefit the formation of an interface by chemically stabilizing the contact interface, removing any highly conductive surface accumulation layer or reducing interfacial trap states.<sup>[8,33–36]</sup> Therefore, a set of new heterojunction diodes with the same structure and materials were fabricated, with plasma surface treatment on a-ZTO before the deposition of Cu<sub>2</sub>O. Nitrogen and oxygen plasmas are used. No post-deposition thermal annealing was done on the diodes.

As shown in **Figure 4a**, the nitrogen-treated diode shows some improvement in current rectification to 100 at 1.0 V, which is a 5× improvement compared to the untreated diode. This arises from the reduction in the reverse current, since the forward current at 1 V is actually ≈10× lower than the untreated diode. Unlike the untreated diode, the nitrogen-treated diode's current increases exponentially between 0 and ≈0.25 V. When fitted using the Shockley diode equation (Equation (1)), the ideality factor extracted is 1.80, which is much improved from that of the untreated diodes. It is also important to note that the nitrogen-treated diode shows a negligible hysteresis in the  $I$ - $V$  sweep.

As shown in **Figure 4b**, the oxygen-treated diode also shows great improved rectifying characteristics of 10 000 at 1.0 V which is an improvement by a factor of ≈500 when compared to the untreated diode. The  $I$ - $V$  characteristics of the oxygen-treated diode maintain a uniform exponential increase in current at low voltage until ≈0.5 V, signifying good junction-limited conduction and negligible parasitic leakage paths. By modeling the  $I$ - $V$  curve using the Shockley diode equation (Equation 1), the ideality factor of the oxygen-treated diode is at 1.53. The reverse current density of the oxygen-treated diode at -1 V is ≈10<sup>-4</sup> A cm<sup>-2</sup>, which is over 100 times lower than the untreated

diode. In contrast to the untreated diode, the oxygen-treated diode shows virtually no hysteresis, especially at forward bias. This may be attributed to the stability of an oxygen-rich material against negative bias stresses (noting the presence of an opposing built-in field at the junction).<sup>[37]</sup>

Plotted in **Figure 4c**, the capacitance of nitrogen-treated diode increases in the forward sweep from -1 to 0.75 V and shows an observable hysteresis in the reverse sweep. The hysteresis is much smaller compared to the untreated diode (**Figure 1c**). The built-in voltage extracted is 0.35 V at 100 kHz (**Figure 4d**). This shows that the nitrogen-treated diode still has a significant quantity of traps present at the interface but in lower concentration compared to the untreated diode (**Figure S2a,c**, Supporting Information). This may also explain why the forward current of the nitrogen-treated diode did not reach similar levels to that of untreated and oxygen-treated diode at ≈1 V, despite having lower reverse current and currents at small applied bias. Overall, the nitrogen-treated diode still exhibits many unwanted characteristics.

On the other hand, the  $C$ - $V$  response of the oxygen-treated diode shows superb characteristics. As shown in **Figure 4c**, it exhibits steady capacitance from -1 to -0.5 V, then a sharp rise from -0.5 to 0.25 V, followed by a sharp fall from 0.25 to 1 V; the  $C$ - $V$  measurements at various frequencies also shows consistent responses at reverse bias (**Figure S2b**, Supporting Information). In **Figure 4d**, the  $C^2$ - $V$  response is linear in almost the entire range of reverse bias; whilst at different frequencies the  $C^2$ - $V$  responses of the oxygen-treated diode exhibits similar properties such as built-in voltage and gradient (**Figure S2d**, Supporting Information). This indicates that the oxygen-treated diode has an abrupt junction, similar to that exhibited by

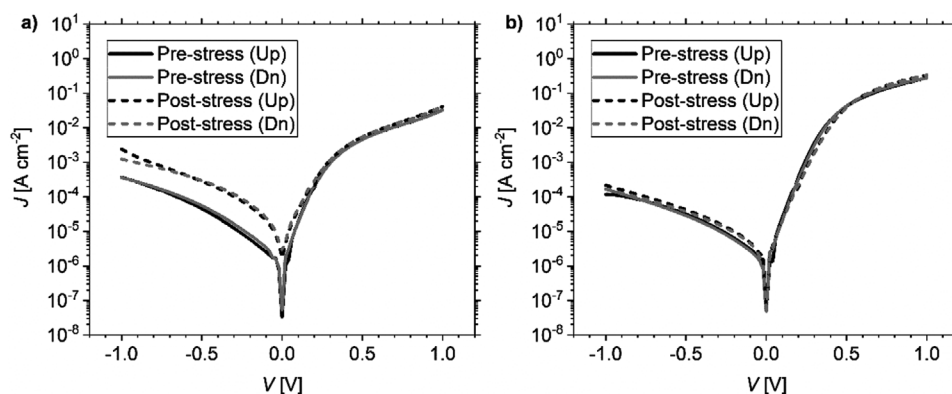


**Figure 5.** Comparison of the  $I$ – $V$  response of the a) nitrogen-treated and b) the oxygen-treated diodes, pre-stress against post-stress. A bias stressing condition of 1 V at 25 °C for 12 h is used.

homojunction diodes. The built-in voltage is  $-0.03$  V at 100 kHz (Figure S2d, Supporting Information). The hysteresis is also very small, further demonstrating the improved performance of the oxygen-treated diode over the untreated one. Overall, the oxygen-treated diode shows significant improvement over both the untreated and nitrogen-treated diodes.

Figure 5a,b shows the  $I$ – $V$  sweep of the nitrogen-treated and oxygen-treated diodes, respectively, done at 25 °C before and after 12 h of bias stress at 1.0 V. The reverse current density of the post-stress nitrogen-treated diode has increased by almost an order of magnitude. On the other hand, the  $I$ – $V$  response of the post-stress oxygen-treated diode has very little difference compared to the pre-stress oxygen-treated diode. The oxygen plasma surface treatment has contributed to a rather stable a-ZTO and  $\text{Cu}_2\text{O}$  interface. It can thus be concluded that nitrogen surface treatment is suboptimal compared to oxygen surface treatment. Table 1 summarizes the parameters extracted from  $I$ – $V$  sweeps for the different diodes.

Hall effect measurements were done on a separate set of a-ZTO thin films in Van der Pauw configuration. Nitrogen and oxygen treatment of the a-ZTO films increased the film resistivity from  $6.1 \times 10^1 \Omega \text{ cm}$  of the untreated film, up to  $8.2 \times 10^3$  and  $4.0 \times 10^5 \Omega \text{ cm}$ , respectively. The carrier mobility increased from  $0.2 \text{ cm}^2 \text{ V}^{-1} \text{ s}^{-1}$  for the untreated film, up to  $10.0 \text{ cm}^2 \text{ V}^{-1} \text{ s}^{-1}$  for the nitrogen-treated films. Due to very high resistivity, the carrier mobility of the oxygen-treated film cannot be determined. On the other hand, the carrier density for the nitrogen- and oxygen-treated films decreased from  $5.0 \times 10^{17}$  for the untreated film, to  $7.5 \times 10^{13}$  and  $6.9 \times 10^{10} \text{ cm}^{-3}$ , respectively. The surface treatments have dramatically increased the film resistivity, with the oxygen plasma massively increasing

resistivity by four orders of magnitude. Because of such large values of resistivity, the error of Hall effect measurement using Van der Pauw configuration is high, but are sufficient to gauge the trend of change. Surface treatments can visibly improve electron mobility, though at the expense of carrier density. This is expected as the passivated traps originated from native donor defects of a-ZTO, that is, oxygen vacancies. Nitrogen plasma seems to have the best balance between increase of resistivity, mobility, and decrease in carrier density. However, this benefit is not reflected in the  $I$ – $V$  responses on the diodes. This could be due to a sizable remaining trap density in the nitrogen-treated a-ZTO, which is a reasonable conclusion based on the Hall effect measurements which illustrated lower resistivity from the higher amount of oxygen vacancies compared to oxygen-treated a-ZTO.

Figure 6a shows X-ray photoelectron spectroscopy (XPS) scans of the differently treated ZTO films. The resolved peaks at  $530.5 \pm 0.52$ ,  $531.5 \pm 0.42$  and  $532.5 \pm 0.73 \text{ eV}$  [38] binding energy show respectively the relative weights of metal–oxygen (M–O) bonds, oxygen anions related to oxygen vacancies ( $\text{V}_\text{O}$ ) and hydroxide (OH) groups, after spectrum shift correction is done based on the adventitious carbon 1s peak at 284.8 eV as reference.[39–42] The compositions of the various XPS peaks of the a-ZTO for the untreated and treated conditions are compared in Figure 6b. The argon treatment does not show any improvement on the film's surface as the peak compositions are very similar between the argon-treated and untreated films. This proves that the benefits of plasma treatment are due to chemical reaction instead of the physical interaction between the plasma and thin film. However, the nitrogen-treated film shows a slight decrease in  $\text{V}_\text{O}$ , which is desirable because too high concentration of oxygen vacancy results in high charge concentration increasing unwanted tunneling at the junction.[8] A further decrease in  $\text{V}_\text{O}$  is observed in the oxygen-treated film, together with an increase in the M–O bonds. The XPS results are consistent with the improvement of the diode performance brought about by the plasma treatment. We hypothesized that the nitrogen plasma surface treatment reduces oxygen vacancies probably by passivating the dangling bonds, as shown previously by the improved stability in the zinc tin oxynitride TFTs.[43] The oxygen plasma treatment shows the benefit of increasing metal–oxygen bonds, in addition to reducing

**Table 1.** Extracted parameters from  $I$ – $V$  responses of different diodes.

	Untreated	$\text{N}_2$ -treated	$\text{O}_2$ -treated
Rectification ratio ( $\pm 1$ V)	$\approx 20$ (1 V)	$\approx 100$ (1 V)	$\approx 10\,000$ (1 V)
Ideality factor	6.45	1.80	1.53
$I_f$ at 1 V [ $\text{A cm}^{-2}$ ]	$4.2 \times 10^{-1}$	$3.3 \times 10^{-2}$	$7.3 \times 10^{-1}$
$I_r$ at $-1$ V [ $\text{A cm}^{-2}$ ]	$3 \times 10^{-2}$	$3 \times 10^{-4}$	$10^{-4}$
$V_{\text{bi}}$ [V]	0.08	0.35	$-0.03$

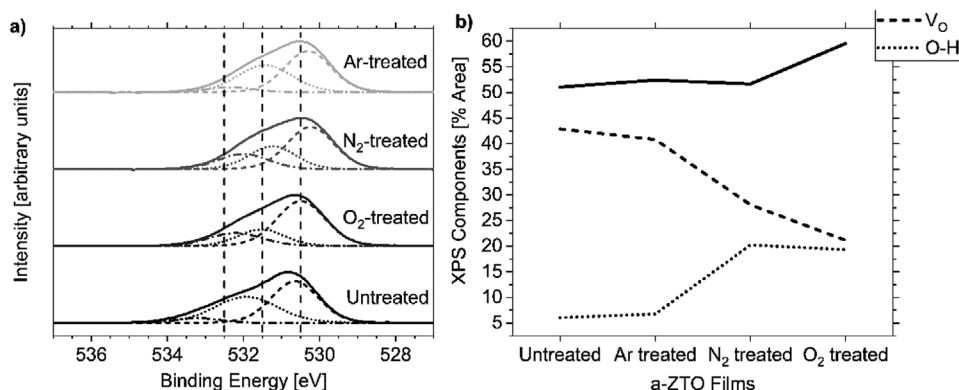


**Figure 6.** a) The overall and resolved XPS scans of the a-ZTO films, untreated and treated under different plasma, b) comparison of the compositions of the XPS peaks of the a-ZTO films in (a).

oxygen vacancies. Due to these chemical changes on the surface, the undesired traps were reduced at the p–n heterojunction and improvements on the diode performance could be observed. This is consistent with many previous investigations on the effect of the oxygen plasma or oxygen annealing treatment to the performance of amorphous oxide semiconductor diodes.<sup>[8,36,39,44–46]</sup> In a previous report on the ZTO Schottky diodes by Schultz et al., an oxidized platinum contact reduced the oxygen vacancy concentration on the ZTO surface of Schottky diodes in an interfacial reaction by oxygen transfer.<sup>[47]</sup> In the present work, the oxygen plasma treatment of the a-ZTO surface achieves similar reduction in oxygen vacancies and thus improves the interface of our p–n heterojunction diodes.

In this specific case, it seems that decreasing oxygen vacancies at the junction is a more crucial factor in improvement of diode performance compared to altering the Fermi levels, though reduced free charge concentration is usually directly linked to shifting of Fermi energy.

**Table 2** compares the device information and the performance of various heterojunction diodes fabricated at room temperature. The performance of diodes produced in this work are comparable to that produced by PLD with the ZTO and zinc cobalt oxide (ZCO) combination, which is the best diode performance reported.<sup>[20]</sup> Therefore, a simple oxygen-treatment and the use of abundant and simple material like Cu<sub>2</sub>O as a p-type material is on par with the all-amorphous heterojunction diode made using PLD. Moreover, the use of sputtering (high target utilisation sputtering (HiTUS) in this case) is hugely beneficial to the large area electronics industry and in general any large-scale manufacturing of electronics because of the scalable process and high deposition rates of sputtering, compared to PLD.<sup>[48]</sup> The performance of diodes produced in this work are also comparable to that of IGZO/Cu<sub>2</sub>O diodes produced by magnetron sputtering at room temperature, where the diodes are operable at high frequencies.<sup>[3]</sup>

**Table 2.** Comparison of reported room-temperature fabricated heterojunction diodes in literature.

Materials	Phase <sup>a)</sup>	Method <sup>b)</sup>	T <sub>fab</sub> (T <sub>max</sub> ) [°C]	Substrate	I <sub>f</sub> /I <sub>r</sub>	η	Ref.
ZCO	a	PLD	RT (90)	Glass	10 <sup>3</sup> –10 <sup>4</sup>	1.2	Schlupp et al. <sup>[20]</sup>
ZTO	a	PLD	RT (90)		(1 V)		
ZCO	a	PLD	RT (90)	Glass	4 × 10 <sup>6</sup>	2.0	Schlupp et al. <sup>[20]</sup>
i-ZTO/ZTO	a	PLD	RT (90)		(1.6 V)		
Cu <sub>2</sub> O	pc	MS	RT	Glass/PEN	3.4 × 10 <sup>4</sup>	1.4	Chen et al. <sup>[3]</sup>
IGZO	a	MS	RT		(1.2 V)		
Cu <sub>2</sub> O	pc	TO	1010	Copper	2 × 10 <sup>3</sup>		Minami et al. <sup>[49]</sup>
ZnO		PLD	RT		(2 V)		
ZnRh <sub>2</sub> O <sub>4</sub>	a	MS	RT	Glass/polyester	10 <sup>3</sup>	2.3	Narushima et al. <sup>[19]</sup>
IGZO	a	MS	RT		(5 V)		
ZCO	a	PLD	RT	Sapphire	10 <sup>2</sup>		Kim et al. <sup>[50]</sup>
IGZO	a	MS	RT		(7 V)		
NiO	c	MS	35 (100)	Polyimide	10 <sup>4</sup>	3.2	Münzenrieder et al. <sup>[2]</sup>
IGZO	a	MS	35 (100)		(2.5 V)		
Cu <sub>2</sub> O	pc	HiTUS	RT (120)	Glass	10 <sup>4</sup>	1.53	This work
ZTO (O <sub>2</sub> treated)	a	HiTUS			(1 V)		

<sup>a)</sup>Phases, a: amorphous, pc: polycrystalline, c: crystalline; <sup>b)</sup>Deposition methods, PLD, pulsed-laser deposition; MS, magnetron sputtering; TO, thermal oxidation; HiTUS, high target utilization sputtering.

### 3. Conclusion

Thin film heterojunction diodes using a-ZTO and Cu<sub>2</sub>O are fabricated and characterized. The n-on-p diode is found to be Ohmic and only the p-on-n diode exhibits rectifying characteristics. The untreated p-on-n diode is functional and rectifying even when vacuum was broken between depositions of the active layers, albeit with a low rectifying ratio of a maximum of 20. *I*-*V* and bias stress measurements of the untreated diode show signs of traps which can be removed to improve the diodes. Oxygen or nitrogen plasma-treating the surface of a-ZTO films shows evidence of increased M-O bonds and reduction of oxygen vacancies and hence improvement in the rectifying performance of the thin film diodes with rectification ratios reaching 10 000. The effect of surface treatments is sufficiently stable to last until the next deposition step and warrants breaking vacuum between depositions. No post-deposition annealing of the films is required to achieve this. The issue of non-rectifying n-on-p diodes may be addressed by similar plasma surface treatments in future work, further increasing the versatility of oxide semiconductor heterojunction diodes.

### 4. Experimental Section

The heterojunction diodes were fabricated on Corning 7059 glass substrates measuring 40 mm × 40 mm. 100 nm thick molybdenum as the bottom contact was sputtered first, then a-ZTO and Cu<sub>2</sub>O of 300 nm thick each were sputtered. Finally, a 60–100 nm gold top contact was thermally evaporated. The diodes were 1 mm × 1 mm in size. The compositions of both oxides along with their X-ray diffraction patterns have been discussed in separate publications.<sup>[9,23]</sup>

Direct current (DC) sputtering on a Metallifier Sputter Coating System (Precision Atomics) was used to deposit molybdenum, with a power of 100 W and argon gas flow rate of 30 sccm. The base pressure was  $5.0 \times 10^{-5}$  mbar. The chamber was kept at  $3.5 \times 10^{-3}$  mbar during the deposition process by automatic gate valve throttling. Reactive sputtering of Cu<sub>2</sub>O and a-ZTO was done in a high-target utilization sputtering (HiTUS) system, with inductively coupled radio-frequency (RF) plasma generated remotely and directed onto the target via a pair of electromagnets (PlasmaQuest Ltd., S500). The plasma has a high ion density typically  $\approx 10^{13}$  cm<sup>-3</sup>, but the ion energy is <50 eV and so the application of a DC target bias is required for sputtering.<sup>[48]</sup> The chamber was pumped down to  $\approx 5.0 \times 10^{-6}$  mbar before depositions, and the chamber pressure was maintained at about  $1.5 \times 10^{-3}$  and  $6.0 \times 10^{-3}$  mbar for Cu<sub>2</sub>O and a-ZTO depositions, respectively. The sputtering targets used for Cu<sub>2</sub>O and a-ZTO are metallic copper and metallic zinc-tin alloy (50 at% Sn), respectively. However, for a-ZTO there seemed to be preferential sputtering of tin atoms, so the resultant film has a higher tin content than the target.<sup>[9]</sup> Launch power and target power for sputtering of a-ZTO were 800 and 500 W, respectively, whilst for Cu<sub>2</sub>O they were 1200 and 1000 W, respectively. The vacuum was broken for roughly 10 min between the a-ZTO and Cu<sub>2</sub>O deposition because of hardware adjustments required by the vacuum system. The depositions were done at room temperature without substrate heating, and the films were not exposed to any post-deposition heat treatment. Evaporation of gold contacts were done in an Edwards E306A thermal evaporation vacuum chamber, at a pressure of  $5 \times 10^{-5}$  mbar, with an average deposition rate of  $\approx 0.15$  nm s<sup>-1</sup>.

After the deposition of the a-ZTO layer, some samples were exposed to nitrogen or oxygen plasma in a custom-made reactive ion etching machine, its chamber measuring  $\approx 21 \times 15 \times 7$  cm. The plasma treatment was performed at a gas flow rate of 100 sccm with a plasma power of 74 W for 1 min. The chamber pressure was kept constant at  $\approx 150$  mBar. The DC bias of nitrogen, oxygen, and argon plasmas were  $\approx 313$ ,  $\approx 350$ ,

and  $\approx 300$  V, respectively. The samples were then returned to the HiTUS chamber for further Cu<sub>2</sub>O deposition and subsequent steps.

In order to measure the electrical resistivity of the untreated and treated a-ZTO or Cu<sub>2</sub>O samples, Mo(Au) contacts were thermally evaporated at the four corners of the a-ZTO(Cu<sub>2</sub>O) films through a shadow mask right after a-ZTO(Cu<sub>2</sub>O) deposition on separate 7 mm × 7 mm glass substrates.

*I*-*V* and *C*-*V* measurements were performed using an Agilent B1500 semiconductor parameter analyzer connected to a Cascade probe station, and bias stress and current-voltage-temperature (*I*-*V*-*T*) measurements were performed on a custom-made probe station with an integrated thermocouple hotplate system connected to an HP4140B pA meter/dual DC voltage source in a dark Faraday's cage. *I*-*V* and *I*-*V*-*T* measurements were carried out with step size of 20 mV, interval between steps of 1 s, swept from -1 to 1 V (up sweep) and then 1 V back to -1 V (down sweep). *C*-*V* measurements were carried out with AC signal of 30 mV at frequencies of 100–300 kHz or as specified, DC step size of 1 mV, step interval of 1 ms, swept up from -1 to 1 V then down to -1 V, similar to *I*-*V* measurements. XPS data were obtained on films deposited on small silicon wafer pieces using ThermoFisher Escalab 250Xi system.

### Supporting Information

Supporting Information is available from the Wiley Online Library or from the author.

### Acknowledgements

The authors would like to thank the EPSRC for support of this project under grant no. EP/M013650/1 and EP/P027032/1, and the Cambridge Trust for supporting the research. Y.J. is a Commonwealth scholar, funded by the UK government.

### Conflict of Interest

The authors declare no conflict of interest.

### Data Availability Statement

Additional data related to this publication is available at the DSpace@Cambridge data repository <https://doi.org/10.17863/CAM.65383>.

### Keywords

amorphous zinc-tin oxide, bipolar devices, cuprous oxide, heterojunction diodes, interface plasma treatments, metal oxides, room temperature high target utilization sputtering (HiTUS)

Received: January 11, 2021  
Revised: February 25, 2021  
Published online: April 1, 2021

- [1] K. Nomura, H. Ohta, A. Takagi, T. Kamiya, M. Hirano, H. Hosono, *Nature* **2004**, *432*, 488.
- [2] N. Münzenrieder, C. Zysset, L. Petti, T. Kinkeldei, G. A. Salvatore, G. Tröster, *Solid-State Electron.* **2013**, *87*, 17.
- [3] W.-C. Chen, P.-C. Hsu, C.-W. Chien, K.-M. Chang, C.-J. Hsu, C.-H. Chang, Wei-Kai Lee, W.-F. Chou, H.-H. Hsieh, C.-C. Wu, *J. Phys. D: Appl. Phys.* **2014**, *47*, 365101.



- [4] K. Nomura, A. Takagi, T. Kamiya, H. Ohta, M. Hirano, H. Hosono, *Jpn. J. Appl. Phys.* **2006**, *45*, 4303.
- [5] H. Hosono, *J. Non-Cryst. Solids* **2006**, *352*, 851.
- [6] J. S. Park, W.-J. Maeng, H.-S. Kim, J.-S. Park, *Thin Solid Films* **2012**, *520*, 1679.
- [7] J.-Y. Kwon, D.-J. Lee, K.-B. Kim, *Electron. Mater. Lett.* **2011**, *7*, 1.
- [8] S. Bitter, P. Schlupp, H. von Wenckstern, M. Grundmann, *ACS Appl. Mater. Interfaces* **2017**, *9*, 26574.
- [9] K. M. Niang, J. Cho, S. Heffernan, W. I. Milne, A. J. Flewitt, *J. Appl. Phys.* **2016**, *120*, 085312.
- [10] S. Han, A. J. Flewitt, *Sci. Rep.* **2017**, *7*, 5766.
- [11] H. Raebiger, S. Lany, A. Zunger, *Phys. Rev. B* **2007**, *76*, 045209.
- [12] Z. Wang, P. K. Nayak, J. A. Caraveo-Frescas, H. N. Alshareef, *Adv. Mater.* **2016**, *28*, 3831.
- [13] H. Ohta, M. Orita, M. Hirano, H. Hosono, *J. Appl. Phys.* **2001**, *89*, 5720.
- [14] H. Ohta, H. Mizoguchi, M. Hirano, *Appl. Phys. Lett.* **2003**, *82*, 823.
- [15] D.-S. Kim, T.-J. Park, D.-H. Kim, S.-Y. Choi, *Phys. Status Solidi A* **2006**, *203*, R51.
- [16] S.-Y. Tsai, M.-H. Hon, Y.-M. Lu, *Solid-State Electron.* **2011**, *63*, 37.
- [17] S. Kim, H. Seok, H. Lee, M. Lee, D. Choi, K. Chai, *Ceram. Int.* **2012**, *38*, S623.
- [18] F.-L. Schein, M. Winter, T. Böntgen, H. von Wenckstern, M. Grundmann, *Appl. Phys. Lett.* **2014**, *104*, 022104.
- [19] S. Narushima, H. Mizoguchi, K. Shimizu, K. Ueda, H. Ohta, M. Hirano, T. Kamiya, H. Hosono, *Adv. Mater.* **2003**, *15*, 1409.
- [20] P. Schlupp, F.-L. Schein, H. von Wenckstern, M. Grundmann, *Adv. Electron. Mater.* **2015**, *1*, 1400023.
- [21] M. Grundmann, R. Karsthof, H. von Wenckstern, *ACS Appl. Mater. Interfaces* **2014**, *6*, 14785.
- [22] A. Sarangan, in *Fundamentals and Applications of Nanophotonics* (Ed.: J.W. Haus), Woodhead Publishing, Cambridge **2016**, pp. 149–184.
- [23] S. Han, K. M. Niang, G. Rughoobur, A. J. Flewitt, *Appl. Phys. Lett.* **2016**, *109*, 173502.
- [24] P. T. Erslev, E. S. Sundholm, R. E. Presley, D. Hong, J. F. Wager, J. D. Cohen, *Appl. Phys. Lett.* **2009**, *95*, 192115.
- [25] P. T. Erslev, H. Q. Chiang, D. Hong, J. F. Wager, J. D. Cohen, *J. Non-Cryst. Solids* **2008**, *354*, 2801.
- [26] A. J. Flewitt, M. J. Powell, *J. Appl. Phys.* **2014**, *115*, 134501.
- [27] W. H. Han, K. J. Chang, *Phys. Rev. Appl.* **2016**, *6*, 044011.
- [28] H.-H. Nahm, Y.-S. Kim, D. H. Kim, *Phys. Status Solidi A* **2012**, *249*, 1277.
- [29] W. Körner, P. Gumbsch, C. Elsässer, *Phys. Rev. B* **2012**, *86*, 165210.
- [30] S. Sallis, K. T. Butler, N. F. Quackenbush, D. S. Williams, M. Junda, D. A. Fischer, J. C. Woicik, N. J. Podraza, B. E. White, A. Walsh, L. F. J. Piper, *Appl. Phys. Lett.* **2014**, *104*, 232108.
- [31] L.-C. Liu, J.-S. Chen, J.-S. Jeng, *Appl. Phys. Lett.* **2014**, *105*, 023509.
- [32] C.-G. Lee, B. Cobb, A. Dodabalapur, *Appl. Phys. Lett.* **2010**, *97*, 203505.
- [33] A. Chasin, S. Steudel, K. Myny, M. Nag, T.-H. Ke, S. Schols, J. Genoe, G. Gielen, P. Heremans, *Appl. Phys. Lett.* **2012**, *101*, 113505.
- [34] J. Kaczmarek, M. A. Borysiewicz, K. Piskorski, M. Wzorek, M. Kozubal, E. Kamińska, *Semicond. Sci. Technol.* **2017**, *33*, 015010.
- [35] B. J. Coppa, C. C. Fulton, S. M. Kiesel, R. F. Davis, C. Pandarinath, J. E. Burnette, R. J. Nemanich, D. J. Smith, *J. Appl. Phys. (Melville, NY, U. S.)* **2005**, *97*, 103517.
- [36] B. J. Coppa, R. F. Davis, R. J. Nemanich, *Appl. Phys. Lett.* **2003**, *82*, 400.
- [37] W.-T. Chen, S.-Y. Lo, S.-C. Kao, H.-W. Zan, C.-C. Tsai, J.-H. Lin, C.-H. Fang, C.-C. Lee, *IEEE Electron Device Lett.* **2011**, *32*, 1552.
- [38] J. Sheng, K.-L. Han, T. Hong, W.-H. Choi, J.-S. Park, *J. Semicond.* **2018**, *39*, 011008.
- [39] M. P. A. Jallorina, J. P. S. Bermundo, M. N. Fujii, Y. Ishikawa, Y. Uraoka, *Appl. Phys. Lett.* **2018**, *112*, 193501.
- [40] P. K. Biswas, A. De, L. K. Dua, L. Chkoda, *Bull. Mater. Sci.* **2006**, *29*, 323.
- [41] T. Ishida, H. Kobayashi, Y. Nakato, *J. Appl. Phys.* **1993**, *73*, 4344.
- [42] J. C. C. Fan, J. B. Goodenough, *J. Appl. Phys.* **1977**, *48*, 3524.
- [43] K. M. Niang, B. C. Bayer, J. C. Meyer, A. J. Flewitt, *Appl. Phys. Lett.* **2017**, *111*, 122109.
- [44] H. L. Mosbacher, Y. M. Strzhemechny, B. D. White, P. E. Smith, D. C. Look, D. C. Reynolds, C. W. Litton, L. J. Brillson, *Appl. Phys. Lett.* **2005**, *87*, 012102.
- [45] A. Chasin, M. Nag, A. Bhoolakam, K. Myny, S. Steudel, S. Schols, J. Genoe, G. Gielen, P. Heremans, *IEEE Trans. Electron Devices* **2013**, *60*, 3407.
- [46] Y. Son, J. Li, R. L. Peterson, *ACS Appl. Mater. Interfaces* **2016**, *8*, 23801.
- [47] T. Schultz, S. Vogt, P. Schlupp, H. von Wenckstern, N. Koch, M. Grundmann, *Phys. Rev. Appl.* **2018**, *9*, 064001.
- [48] A. J. Flewitt, J. D. Dutson, P. Beecher, D. Paul, S. J. Wakeham, M. E. Vickers, C. Ducati, S. P. Speakman, W. I. Milne, M. J. Thwaites, *Semicond. Sci. Technol.* **2009**, *24*, 085002.
- [49] T. Minami, Y. Nishi, T. Miyata, *Appl. Phys. Express* **2013**, *6*, 044101.
- [50] S. Kim, J. A. Cianfrone, P. Sadik, K.-W. Kim, M. Ivill, D. P. Norton, *J. Appl. Phys.* **2010**, *107*, 103538.